Salvador Vargas, Carmen Vázquez (2014). "Optical Reconfigurable Demultiplexer Based on Bragg Grating Assisted Ring Resonators". In Optics Express, Volume: 22, Issue: 16, Pages: 19156–19168. Available in http://dx.doi.org/10.1364/OE.22.01914119156

Optical reconfigurable demultiplexer based on Bragg grating assisted ring resonators

Salvador Vargas[1,2,*] and Carmen Vazquez[1]

[1]*Department of Electronic Technology, Universidad Carlos III de Madrid, Ave. Universidad No. 30, C.P: 28911, Leganés, Madrid, Spain*

[2]*Electrical Engineering Faculty, Universidad Tecnológica de Panamá, Ave. Universidad Tecnológica, El Dorado 0819-07289, Panamá, Panama*

[*]*salvador.vargas@utp.ac.pa*

Abstract: A polarization independent reconfigurable optical demultiplexer with low crosstalk between adjacent channels and high number of potential allocated channels is designed on silicon on insulator technology. On to off state transitions can be implemented by changing the coupling factor or the ring length. Wavelength selective switch units are cascaded to form the demultiplexer. Crosstalks below −30dB with 50GHz channel spacing and losses below 1.5dB in the off state are obtained from simulations. Designs using carrier dispersion effect and power consumption estimations are included.

References and links

1. H. Zang, J. P. Jue, and B. Mukherjeea, "Review of Routing and Wavelength Assignment Approaches for Wavelength-Routed Optical WDM Networks," Opt. Netw. Mag. **1**, 47–60 (2000).
2. T. E1-Bawab, *Optical Switching* (Springer, 2010).
3. I. Kiyat, A. Aydinli, and N. Dagli, "Low-Power Thermooptical Tuning of SOI Resonator Switch," IEEE Photon. Technol. Lett. **18**(2), 364–366 (2006).
4. E. J. Klein, P. Urban, G. Sengo, L. T. H. Hilderink, M. Hoekman, R. Pellens, P. van Dijk, and A. Driessen, "Densely integrated microring resonator based photonic devices for use in Access networks," Opt. Express **15**(16), 10346–10355 (2007).
5. S. J. Emelett and R. A. Soref, "Analysis of dual-microring-resonator cross-connect switches and modulators," Opt. Express **13**(20), 7840–7853 (2005).
6. R. Boeck, N. A. F. Jaeger, N. Rouger, and L. Chrostowski, "Series-coupled silicon racetrack resonators and the Vernier effect: theory and measurement," Opt. Express **18**(24), 25151–25157 (2010).
7. F. Xia, M. Rooks, L. Sekaric, and Y. Vlasov, "Ultra-compact high order ring resonator filters using submicron silicon photonic wires for on-chip optical interconnects," Opt. Express **15**(19), 11934–11941 (2007).
8. Y. Zhang, P. Chowdhury, M. Tornatore, and B. Mukherjee, "Energy Efficiency in Telecom Optical Networks," IEEE Commun. Surveys Tuts. **12**(4), 441–458 (2010).
9. L. Shuai, W. Yuanda, Y. Xiaojie, A. Junming, L. Jianguang, W. Hongjie, and H. Xiongwei, "Tunable filters based on an SOI nano-wire waveguide micro ring resonator," J. Semiconduc. **32**, 084007 (2011).
10. R. Soref and B. Bennett, "Electrooptical Effects in Silicon," IEEE J. Quantum Electron. **23**(1), 123–129 (1987).
11. Q. Xu, B. Schmidt, S. Pradhan, and M. Lipson, "Micrometre-scale silicon electro-optic modulator," Nature **435**(7040), 325–327 (2005).
12. C. Li, L. Zhou, and A. W. Poon, "Silicon microring carrier-injection-based modulators/switches with tunable extinction ratios and OR-logic switching by using waveguide cross-coupling," Opt. Express **15**(8), 5069–5076 (2007).
13. P. Dong, W. Qian, H. Liang, R. Shafiiha, X. Wang, D. Feng, G. Li, J. E. Cunningham, A. V. Krishnamoorthy, and M. Asghari, "1x4 reconfigurable demultiplexing filter based on free-standing silicon racetrack resonators," Opt. Express **18**(24), 24504–24509 (2010).
14. S. Vargas and C. Vazquez, "Synthesis of optical filters using microring resonators with ultra-large FSR," Opt. Express **18**(25), 25936–25949 (2010).
15. C. Vázquez, S. Vargas, and P. Contreras, "Low power consumption in silicon photonics tuning filters based on compound ring resonators," in Silicon Photonics VIII, Photonics West, Proc. SPIE **8629**, 44–50 (2013).
16. D. Dai, J. Bauters, and J. E. Bowers, "Passive technologies for future large-scale photonic integrated circuits on silicon: polarization handling, light non-reciprocity and loss reduction," Light: Sci. Appl. **1**(3), 1–14 (2012).
17. S. Ghosh, S. Keyvaninia, W. Van Roy, T. Mizumoto, G. Roelkens, and R. Baets, "Adhesively bonded Ce:YIG/SOI integrated optical circulator," Opt. Lett. **38**(6), 965–967 (2013).

18. C. Vázquez, S. Vargas, J. M. S. Pena, and P. Corredera, "Tunable Optical Filters Using Compound Ring Resonators for DWDM," IEEE Photon. Technol. Lett. **15**(8), 1085–1087 (2003).
19. J. G. Proakis and D. G. Manolakis, *Digital Signal Processing*, (Pearson Prentice Hall, 2006).
20. Y. A. Vlasov and S. J. McNab, "Losses in single-mode silicon-on-insulator strip waveguides and bends," Opt. Express **12**(8), 1622–1631 (2004).
21. S. P. Chang, C. E. Png, S. T. Lim, V. M. N. Passaro, and G. T. Reed, "Single mode and polarization independent SOI waveguides with small cross section," J. Lightwave Technol. **23**, 1573–1582 (2005).
22. W. Headley, G. Reed, S. Howe, A. Liu, and M. Paniccia, "Polarization-independent optical racetrack resonators using rib waveguides on silicon-on-insulator," Appl. Phys. Lett. **85**(23), 5523–5526 (2004).
23. F. Sun, J. Yu, and S. Chen, "Directional-coupler-based Mach-Zehnder interferometer in silicon-on-insulator technology for optical intensity modulation," Opt. Eng. **42**, 25601–25605 (2007).
24. P. Dong, S. Liao, H. Liang, R. Shafiiha, D. Feng, G. Li, X. Zheng, A. V. Krishnamoorthy, and M. Asghari, "Submilliwatt, ultrafast and broadband electro-optic silicon switches," Opt. Express **18**(24), 25225–25231 (2010).
25. J. Dziewior and W. Schmid, "Auger coefficients for highly doped and highly excited silicon," Appl. Phys. Lett. **31**(5), 346–348 (1977).
26. M. Hossein-Zadeh and K. J. Vahala, "Optomechanical Oscillator on a Silicon Chip," IEEE J. Sel. Top. Quantum Electron. **16**(1), 276–287 (2010).

1. Introduction

Wavelength-Division Multiplexing (WDM) in optical fiber networks has been rapidly gaining acceptance as a means to handle the ever-increasing bandwidth demands of network users. In a wavelength-routed WDM network, end users communicate with one another via all-optical WDM channels, which are referred to as lightpaths. Wavelength selective optical switches are needed to set up lightpaths at different wavelengths [1].

There are several types of optical switches depending on the fabrication technologies used to construct them, like lithium niobate, acousto-optic, thermo-optic, liquid crystal, micro-electromechanical systems (MEMS), semiconductor optical amplifiers (SOA) and ring resonators (RR) [2].

From all these types, the RR WDM switches are very versatile as they can be integrated with other devices using integrated optics technology, like silicon on insulator (SOI) technology. This technology permits the maximum integration due to its high refractive index contrast. These WDM switches have applications working individually [3], or as part of optical multiplexers/demultiplexers [4], optical routers and optical cross connects [5]. Nevertheless, because of its periodic transfer function the number of channels they can switch is limited by its free spectral range (FSR).

To avoid this restriction, it has been proposed structures using the Vernier effect [6] to increase the FSR. Also to improve the on-off ratio and reduce the crosstalk have been cascaded RR to realize higher order transfer functions [7], although this technique increase the footprint in the wafer in the integrated optics device.

On the other hand, due to the rapid growth of energy consumption in ICT (Information and Communication Technologies), lot of attention is being devoted towards "green" ICT solutions [8]. Energy consumption in optical networks will be reduced by using components consuming a lower amount of energy.

In RR based WDM switches most of the power is consumed to switch and maintain any optical path change, which induce a commutation of the WDM switch state. This optical path change can be done by means of the thermo-optic effect [3, 9], or by mean of electro-optical effects like electric field or charge carrier effects [10–12]. To save energy it has been designed structures with free standing waveguides with undercut structures [13] highly efficient, which significantly reduces the tuning power.

In this paper, we propose and design a reconfigurable optical demultiplexer based on RR WDM switches technology, assisted with Bragg Gratings (BG). Simulations to describe its features are reported. The demultiplexer is composed by individual WDM switches tuned to proper wavelengths. Avoiding the restriction imposed by the periodic function of the RR with a non periodic transfer function inside the ring [14], the BG. The number of channels to be demultiplexed can be increased beyond the limit of a single RR FSR, by cascading more WDM switches. The crosstalk and on off ratio are also, decreased and increased respectively,

in comparison with the demultiplexers based on single RRs, as the basic unit of the switch has a second order transfer function. It can provide a similar performance to demultiplexers based on double RR, but using a smaller footprint with greater manufacturing tolerance as they operate with only one physical ring [15].

Finally, two control mechanisms are analyzed, the change in the coupling factor and the change in the ring optical path length.

2. WDM Switches

N WDM switch units, as the one shown in Fig. 1, can be cascaded to form the demultiplexer. This basic unit is a RR BG assisted WDM switch. There is one of these units by each wavelength to demultiplex and being tuned at a specific information channel frequency.

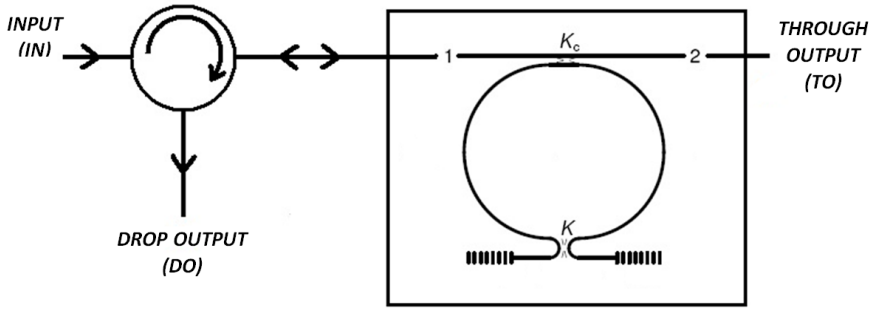

Fig. 1. WDM switch unit.

The basic unit, see Fig. 1, consists of a RR with a Michelson interferometer (MI) placed inside. The MI is made of a directional coupler, with coupling factor *K* and identical BGs as frequency selective mirrors. The BG central frequency is tuned to the frequency of the maximum RR transfer function amplitude, the information channel frequency. The basic unit has also a circulator to redirect the signal reflected from the ring to the drop output port. Optical circulators and isolators are non-reciprocal optical devices. Optical isolators based on ring resonators have already being manufactured using a special bonding technology to combine magneto optic materials with silicon integrated photonic circuits [16]. Recently, 3-port optical circulators in a SOI compatible fabrication process based on a Mach-Zehnder interferometer were reported in [17].

The most important part of the basic unit is the RR with a Michelson interferometer (RRMI). The MI acts as a transmitting-reflecting function allowing the clockwise and counterclockwise propagation of light inside the ring. There are two outputs for the RRMI, the through output (TO) and the drop output (DO), because of this double recirculation. Both are second order transfer functions, non-periodic in frequency, due to the BG transfer function. This configuration permits lower crosstalk than a single RR placed in series with a BG [14].

The transfer functions of the RRMI can be calculated using the transfer matrix formalism in the z domain [18]:

$$\frac{A_2}{A_1} = \frac{(1-\gamma_c)^{1/2}\left(1-Z_{c1}z^{-1}\right)\left(1-Z_{c2}z^{-1}\right)}{\left(1-Z_{p1}z^{-1}\right)\left(1-Z_{p2}z^{-1}\right)} \tag{1}$$

$$\frac{A_{1R}}{A_1} = \frac{j(1-\gamma_c)(1-\gamma)K_c(1-2K)\left|r(\Omega)\right|e^{-\alpha L}z^{-1}}{\left(1-Z_{p1}z^{-1}\right)\left(1-Z_{p2}z^{-1}\right)} \tag{2}$$

where A_2/A_1 and A_{1R}/A_1, are the TO and DO transfer functions respectively, where $(1-\gamma_c)$, K_c and $(1-\gamma)$, K are the excess loss coefficient and coupling factors of the input and MI couplers respectively; $/r(\Omega)/$ is the BG modulus, α is the attenuation coefficient of the waveguides and

L is the round trip length in the ring. Z_{c1} and Z_{c2} are the zeroes of the through transfer function:

$$Z_{c1} = \frac{(1-\gamma_c)^{1/2}(1-\gamma)|r(\Omega)|e^{-\alpha L}}{(1-K_c)^{1/2}}\left[-j\left((1-K_c)(1-2K)^2 - K_c^2\left(K-K^2\right)\right)^{1/2} + (2-K_c)\left(K-K^2\right)^{1/2}\right] \quad (3)$$

$$Z_{c2} = \frac{(1-\gamma_c)^{1/2}(1-\gamma)|r(\Omega)|e^{-\alpha L}}{(1-K_c)^{1/2}}\left[j\left((1-K_c)(1-2K)^2 - K_c^2\left(K-K^2\right)\right)^{1/2} + (2-K_c)\left(K-K^2\right)^{1/2}\right] \quad (4)$$

Z_{p1} and Z_{p2} are the complex conjugated poles of both transfer functions and their modulus and phase are given by:

$$\left|Z_p\right| = (1-\gamma)\left[(1-\gamma_c)(1-K_c)\right]^{1/2}\left|r(\Omega)\right|e^{-\alpha L} \quad (5)$$

$$\varphi_p = \pm\tan^{-1}\left[\frac{(1-2K)}{2\sqrt{\left(K-K^2\right)}}\right] \quad (6)$$

All transfer function simulations are based on Matlab software.

2.1 Transfer function discussion

The drop output, see Eq. (2) has a fix zero at the origin. The zeroes of the through transfer function, see Eq. (1), can be placed at different positions in the Z plane by means of the change in the coupling factors K and K_c. The modulus of these zeroes can be complex conjugated, or real and they can be different depending on the values of K and K_c. The zeroes are complex conjugated if K_c is smaller than K_{lim}:

$$K_{\lim} = \begin{cases} \dfrac{1-2K}{1-K} & 0 \le K < 0.5 \\ \dfrac{2K-1}{K} & 0.5 < K \le 1 \end{cases} \quad (7)$$

Otherwise, the zeroes are real positives and different.

In Fig. 2, see the zeroes modulus of the RRMI through transfer function evolution versus the K_c factor, at a fix K. This modulus is less than 1 for complex zeroes and its value greatly increase for real zeroes, see Eq. (3). This property of the through transfer function can be used to control the WDM switch status.

If a zero of any transfer function is mapped onto the unit circle line, the transfer function magnitude is zero at the frequency that corresponds to an angle given by the zero phase [19]. Then by placing a zero of the through transfer function, given in Eq. (1), at the unit circle line, the signal amplitude at the frequency that corresponds to the angle given by this zero phase, in this case the information channel frequency, is highly attenuated. From Fig. 2, this can be fulfilled adjusting K_c to a value slightly higher than K_{lim}, where the modulus of the zero is 1.

For proper operation of the WDM switch, the same frequency channel at the drop output need to be dropped, see Eq. (2). The pole phases must be equal to 0, or to the nearest possible value. This is fulfilled when K equals 0.5, see Eq. (6), but in this case the transmitting-reflecting function becomes only a transmitting function. Because of this a K value of 0.49 is chosen for this coupler in the basic unit.

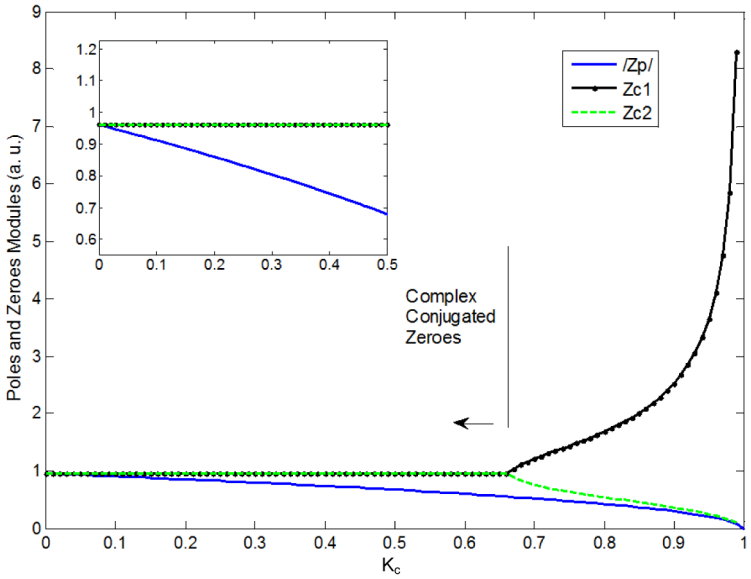

Fig. 2. Poles and Zeroes Modulus of the RRMI through transfer function, with K = 0.25, $\gamma = \gamma_c$ = 0.025 and losses in the RR less than 0.01 dB.

For the chosen K value of 0.49 the corresponding K_{lim} is 0.0392, see Eq. (7). In this case, the switch is working at the *on* state, the frequency channel at which the switch is tuned, is rejected at the through output and dropped at the drop output.

For the *off* state, the channel rejection on the through output must be avoided. A way to fulfill this is by cancelling the zeroes with the poles of the through transfer function, to have an all pass filter response. The modulus and phases of the complex conjugated zeroes of the through transfer function [18] are given by:

$$\left|Z_c\right| = \left(1-\gamma_c\right)^{1/2}\left(1-\gamma\right)\left|r(\Omega)\right| e^{-\alpha L} \tag{8}$$

$$\varphi_c = \pm\tan^{-1}\left(\frac{\left(\left(1-K_c\right)\left(1-2K\right)^2 - K_c^{\,2}\left(K-K^2\right)\right)^{1/2}}{\left(2-K_c\right)\sqrt{K-K^2}}\right) \tag{9}$$

From Eqs. (5)-(6) and Eqs. (8)-(9), it can be seen that they are canceled for K_c values tending to 0, where $|Z_p| \approx |Z_c|$ and $|\varphi_p| \approx |\varphi_c|$. In this design a K_c value of 0.01 is taken.

Switching from the *off* to the *on* state can be achieved by changing the coupling factor K_c from 0.01 to a higher value that depends on K, BG, ring losses and the desired crosstalk between channels.

By changing the optical path in the ring, this switching from *off* to *on* can also be achieved.

2.2 Waveguides design

A design on a SOI platform is going to be performed, its high index contrast enables better mode confinement and smaller bending radius, increasing the integration density against others technologies.

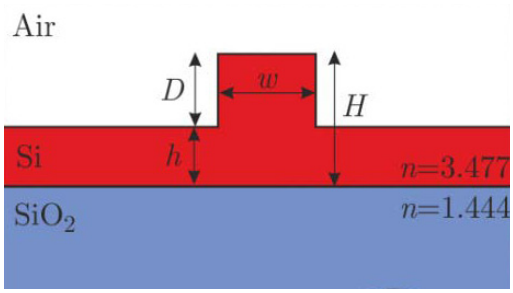

Fig. 3. Schematic layout of the proposed rib waveguide with w = 0.67 μm, H = 1 μm and D = 0.62 μm.

Other design constraint is that the waveguides need to be single mode and polarization independent. The single mode condition is more difficult to fulfill in strip type waveguides because the cross sectionals dimensions must be significantly smaller than 1 μm^2. The roughness of the side walls is very important at these dimensions because it increases the losses for TE mode [20], and the device will be polarization dependent. The single mode condition is more relaxed by using rib waveguides with surface cladding of air with width (w) and height (H) on the order of 1 μm. The dimensions of the waveguides are chosen to have a single mode and zero birefringence waveguide [21-22]. From simulations using a FDTD-based FullWAVE software from RSoft, a rib waveguide with w = 0.67 μm, H = 1 μm and etch depth (D) of 0.62 μm, is selected see Fig. 3.

3. WDM switch control

WDM switch control can be done by changing the coupling factor K_c, or the ring resonator optical path. In any case, a coupler with a specific coupling coefficient has to be designed. In the first case, it is also necessary to design a variable coupler.

A variable coupler based on a Mach-Zehnder (MZ) configuration as in [23] is not adequate, because of the different arms lengths of the interferometer with various delay paths from the input to the output. This affects the frequency response of the device in a complex form. A variable directional coupler (DC) with a p-i-n configuration in one of the DC waveguides is selected. By changing the refractive index, the propagation constants of the waveguides are desynchronized, and the coupling factor changes. The coupling factor of a DC at desynchronism is given by:

$$K_c = \sin^2\left(\delta\sqrt{1+\left(\frac{\xi}{\delta}\right)^2}\right)\left(\frac{1}{1+\left(\frac{\xi}{\delta}\right)^2}\right) \tag{10}$$

where $\delta = \kappa \cdot L_C$, being κ the coupling coefficient, and L_C the length of the coupler, ξ is given by $\Delta\beta \cdot L_C/2$, where $\Delta\beta = \beta_1 - \beta_2$, is the difference between the propagation constants at the two waveguides of the coupler.

At synchronism $\xi = 0$, and the coupling factor K_c is given by:

$$K_c = \sin^2\left(\kappa \cdot L_C\right) \tag{11}$$

At synchronism, the WDM switch is at *on* state.

A polarization independent directional coupler is designed using a RSoft's BeamPROP software tool. Simulations at both polarizations are shown in Figs. 4(a) and 4(b). A waveguide separation of 0.067 μm is considered.

From Fig. 4, it can be seen that the necessary length for complete optical power transfer between waveguides is $L_{\pi/2}$ = 11.75 μm. From this parameter and using Eq. (11), κ = 133684.8 m^{-1} is obtained.

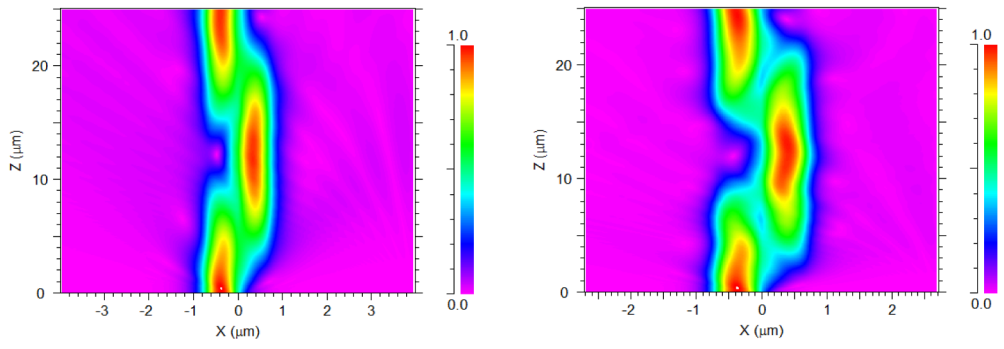

Fig. 4. Polarization independent directional coupler: a) TE polarization and b) TM polarization. Cross section of the waveguides is shown in Fig. 3.

From Eq. (10) it can be concluded that the state of the WDM switch at synchronism is *on*, because it needs the larger coupling factor. This coupling factor K_c, in the *on* state can be extracted from the expected crosstalk for adjacent channels. In Fig. 5 there is a simulation of the switch crosstalk at the through output versus K_c for 50 GHz, and 25 GHz channel separations. The WDM switch parameters are a total length L of 100 μm, $\gamma = \gamma_c = 0.025$, 0.5 dB/cm waveguide losses and a BG maximum reflectivity of 1. The minimum crosstalk is found for K_c value of 0.0841, the value that places the zero at the unitary circle. For crosstalks lower than −50dB, the coupling factor in the *on* state should be in the vicinity of 0.0841. Crosstalk lower than −30 dB for channel spacing of 25 GHz and 50 GHz, can be obtained for this design with $K_c = 0.08$.

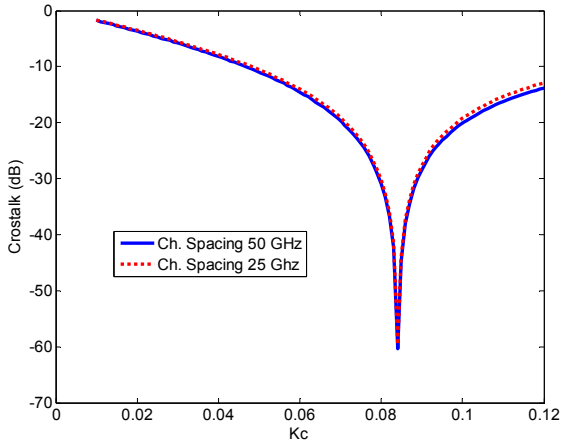

Fig. 5. Crosstalk for adjacent channels with separations of 50 GHz, and 25 GHz.

The coupling length of the first coupler to get $K_c = 0.08$ is found from Eq. (11), which results in $\delta = 2.8548$. Here we take the second zero because it minimizes the ξ ($\Delta\beta$) change needed to switch the state, due to the fact that the two factors in Eq. (10) are decreasing functions at this point. As κ is already calculated, this results in a coupler length $L_C = 21.36$ μm.

The next step is to find the refractive index change (Δn) needed to switch from *on* to *off* state. This can be found solving numerically Eq. (10) with $K_c = 0.01$, to find the ξ and then the needed change between the propagation constants of the coupler ($\Delta\beta$). This results in $\xi = 1.03044$ and $\Delta\beta = 0.9948 \times 10^5$ m^{-1}. The relation of $\Delta\beta$ vs Δn is approximately linear, as it can be seen in Fig. 6 at 1550 nm, and the Δn needed is −0.0236.

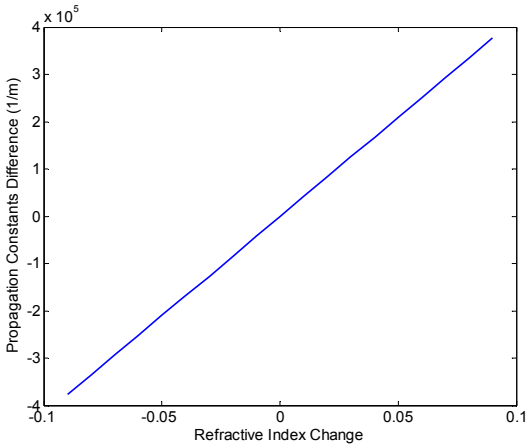

Fig. 6. Dependence of $\Delta\beta$ with Δn for the proposed waveguides at 1550 nm.

The waveguide refractive index (Δn) and losses ($\Delta\alpha$ (Np/cm)) change depends on the carrier concentration. They are given by [10]:

$$\Delta n = -8.8\times10^{-22}\Delta N_e - 8.5\times10^{-18}\left(\Delta N_h\right)^{0.8} \tag{12}$$

$$\Delta\alpha = 8.5\times10^{-18}\Delta N_e + 6\times10^{-18}\Delta N_h \tag{13}$$

where ΔN_e and ΔN_h the change in the electrons and holes concentrations in cm^{-3}.

From Eq. (12) with a $\Delta N_e = \Delta N_h = \Delta N$ and solving numerically for $\Delta n = -0.0236$, we derive a carrier concentration change of $\Delta N = 1.068 \times 10^{19}$ cm^{-3}. It is in the margin of carrier concentration from 10^{17} to 10^{20} cm^{-3}, where Eq. (12) and Eq. (13) are applicable [24].

Finally, optical loss changes due to the carrier concentration injection are found using Eq. (13), being $\Delta\alpha = 154.86$ Np/cm. For a coupler length of 21.36 μm, this change represents 1.4 dB of attenuation at the upper waveguide of the coupler. This attenuation appears only at the *off* state. It can be treated as an insertion loss of 2 × (1.4) dB at the drop output transfer function, and an insertion loss of 1.4 dB at the through output transfer function.

In the case of changing the optical path in the ring, by injecting free carriers on a length of 80 μm, we need to produce a $\Delta\beta = \pi/80\mu$. From Fig. 6, we need a $\Delta n = 0.009378$, which means a $\Delta N = 3.71 \times 10^{18}$ cm^{-3}; so lesser optical losses can be obtained.

3.1 Spectral response

The spectral responses of both outputs of the WDM switch at the *on* state are shown in Figs. 7(a) and 7(b). The parameters on those simulations are: $\gamma = \gamma_c = 0.025$, $\alpha = 0.5$ dB/cm, $L = 100$ μm, and BG maximum reflectivity of 1, $K = 0.49$ and $K_c = 0.08$.

As we can see in Figs. 7(a) and 7(b), an attenuation of 34 dB and 12 dB for the center frequency f_0 of the channel, at the through and drop output respectively and a crosstalk −37 dB for 50 GHz channel spacing, at the drop output are obtained. For the through output, the rest of frequency channels are attenuated a maximum of 0.5 dB, having a rejection bandwidth at 3 dB of 23 GHz, and of 8.32 GHz at 10 dB. In the drop output, there is a full width at half maximum (FWHM) of 16.2 GHz. These bandwidths can be increased without changing the spectral responses only by decreasing the light transit time in the RR.

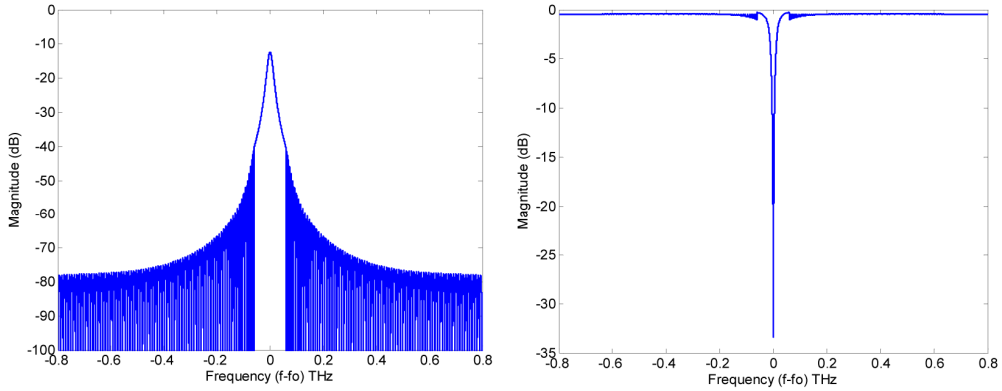

a) b)

Fig. 7. WDM switch spectral response simulations at *on* state, of the drop a), and through b) outputs.

In Figs. 8(a) and 8(b) are shown the spectral responses of the WDM switch at the *off* state. There is an attenuation of 24 dB for the tuned channel frequency at drop output, 12 dB more than in the *on* state, and a FWHM of 10 GHz, 6 GHz less than in the *on* state. In the through output, there is a maximum attenuation of 3.4 dB for the tuned channel frequency f_0, while the others channels are attenuated a maximum of 1.6 dB, due to the coupler waveguide losses.

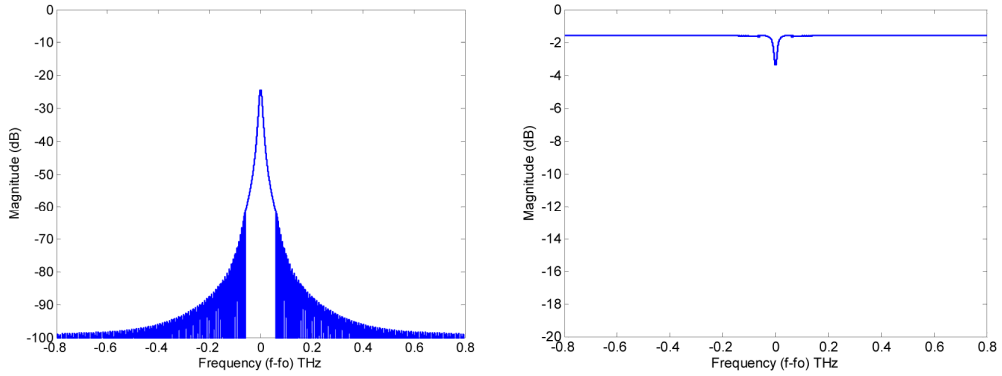

a) b)

Fig. 8. WDM switch spectral response, at *off* state on the drop a), and through b) outputs.

3.2 Power consumption

The switching of the basic unit is obtained by forward biased of a p-i-n diode, either on the coupler waveguides or in the loop length. The current needed for the free carrier change $\Delta N_e = \Delta N_h = \Delta N$, is given by [24]:

$$I = \frac{\Delta N \, e \, S \, L_c}{\tau} \tag{14}$$

where τ is the free carrier recombination time, e is the electron charge, S is the silicon area of the waveguide cross section and L_C is the coupler length. S can be found from the distribution of the waveguide mode profile obtained from RSoft's BeamProp tool, see Fig. 9. Then S is approximated to 0.75 μm^2, the area of the trapezoid shown at Fig. 9 in dashed lines.

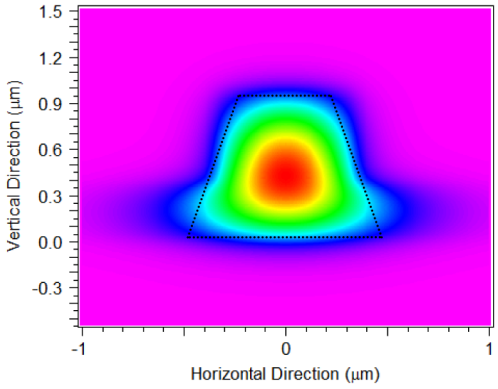

Fig. 9. Transverse mode profile.

The recombination time can be obtained from the electrons and holes recombination rate which have three components, the band to band, the trap assisted or SRH (Shockley, Read and Hall) and the Auger recombination. In Silicon, for carrier or doping concentrations higher than 1×10^{17} cm^{-3}, the recombination rate is dominated by the Auger process [25], which is given by:

$$R_{Aug} = \left(C_n n + C_p p\right)\left(np - n_i^2\right) \tag{15}$$

where the C_n and C_p are the Auger coefficients for electrons and holes recombination, with approximated values of 2.8×10^{-31} cm^6/s and 9.9×10^{-32} cm^6/s respectively [25]; n and p are the concentrations of electrons and holes, and n_i is the intrinsic concentration and could be neglected.

The recombination time is given by:

$$\tau = \frac{\Delta N}{R_{Aug}} \tag{16}$$

In the coupling coefficient change case ΔN, and L_C are equal to 1.068×10^{19} cm^{-3} and 21.36 µm respectively, From Eq. (15) it is obtained that R_{Aug} is equal to 4.617×10^{26} cm^{-3}s^{-1} and τ = 23.13 ns, a time in the order of ns as the one measured in [24]. From Eq. (14) the current needed depends on the recombination time τ and is given by $I = 2.7409 \times 10^{-11}/\tau$ so it is equal to 1.18 mA.

In the case of changing the optical path in the ring, the needed ΔN is 3.71×10^{18} cm^{-3}, therefore a current of 0.14 mA for the *off* state.

The change of the coupling factor can also be done as in optomechanical oscillators [26], which could lead to smaller losses and power consumptions.

4. WDM demultiplexer

Four WDM switches are cascaded to form a 1x4 WDM demultiplexer. Each switch is tuned at a different channel, see Fig. 10. Each frequency channel can be routed to its corresponding drop output or it can be passed to the through output depending on the state of each one of the WDM switches.

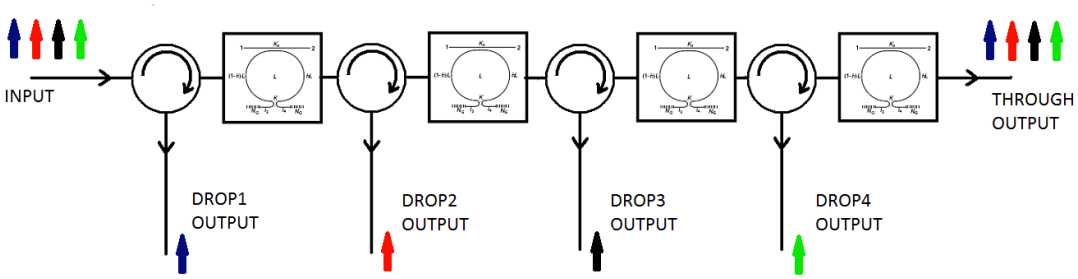

Fig. 10. 1x4 WDM demultiplexer, with each WDM Switch tuned to different wavelengths.

When all the WDM switches are at the *off* state, a total consumption of 4 times the consumption of each WDM switch is expected. In this state, all WDM switches pass all the channel frequencies to the through output. In Figs. 11(a) and 11(b), can be seen the through output and the four drop outputs for a 50 GHz channel spacing and being the x-axis referred to fc, the center frequency of the information channels band of the demultiplexer.

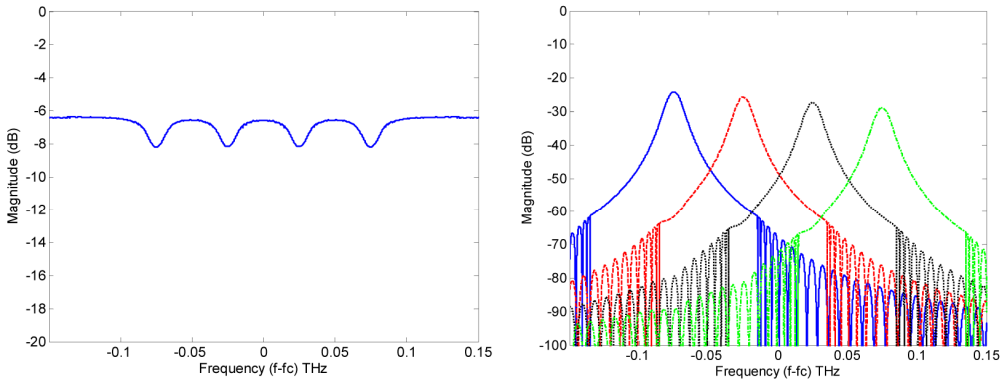

Fig. 11. Spectral response of WDM demultiplexer with all the WDM switches at the *off* state. Through output a) and the four drop outputs b).

In the following the tuning of the device by changing the coupling coefficient through carrier injection, as reported in section 3.

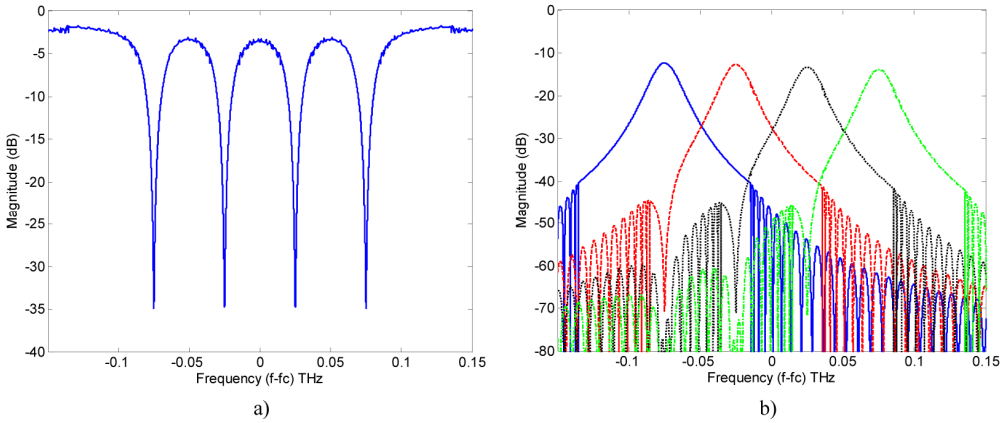

Fig. 12. Spectral response of WDM demultiplexer with all the WDM switches at the *on* state. Through output a) and drop outputs b).

The maximum attenuation expected at the through output is given when all the switches are at the *off* state. In this case, each one contributes to the insertion loss with 1.59 dB, so a total attenuation of 6.36 dB, in the frequency bands out of the information channels band, as we can see in Fig. 11(a). And an attenuation higher than 24 dB for all channel frequencies at the drop outputs of the demultiplexer. There is an attenuation increase of 1.67 dB at each successive stage, see Fig. 11(b).

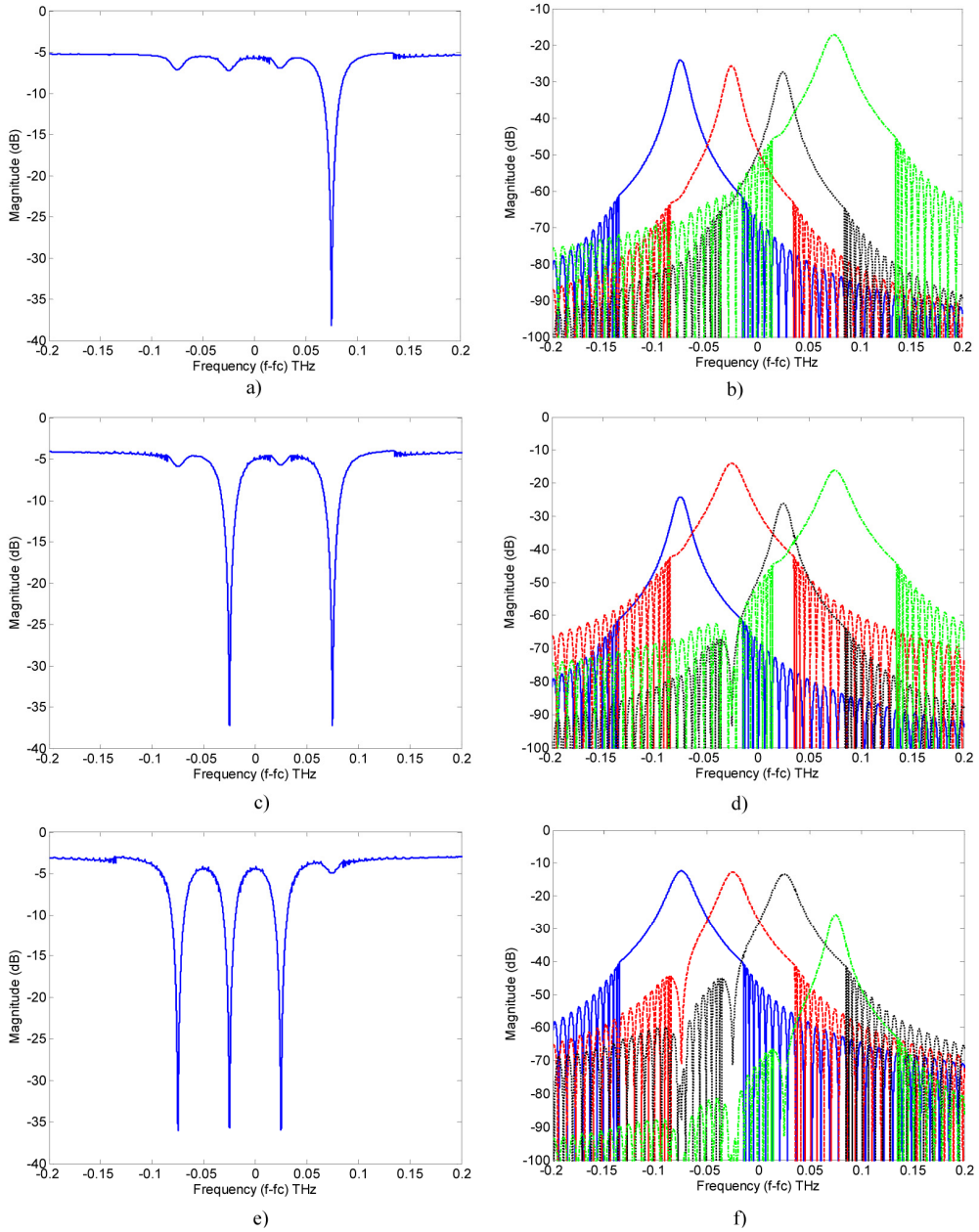

Fig. 13. Spectral response of WDM demultiplexer: for one (fourth) channel extracting a) through output b) drop outputs. For two (second and fourth) channels extracting c) through output d) drop outputs. For three (first, second and third) channels extracting e) through output f) drop outputs.

Another special case to be analyzed is when all the switches are at the *on* state. In this case, the through output rejects all the channels, and each channel is extracted by its drop output. The spectral response for this case is shown in Fig. 12.

From Fig. 12(a), can be seen a rejection of −35 dB, for each of the four frequency channels at the through output. And from Fig. 12(b), can be seen that the crosstalk is lower than −37 dB at the drop port, with a FWHM of 16.2 GHz. For the drop outputs we have an attenuation increasing by 0.2 dB at each successive stage. This value is less than the one obtained for all the switches at *off* state because the losses due to free carrier injection are not present. Also from Fig. 11 and Fig. 12, we can extract the *on off* ratio parameter being of 27 dB and 12 dB for the through and drop output respectively.

Finally we explore some examples when one, two and three frequency channels are extracted at the drop outputs. In Figs. 13(a)–13(f) are shown through and drop outputs for those examples.

The attenuation of the frequency bands out of the information channels decreases for each extracted channel, being respectively 5.2 dB, 4.1 dB and 3 dB for one, two and three extracted channels, see Figs. 13(a), 13(c) and 13(e). This is because for each non extracted channel there is one extra WDM switch at the *off* state, with an extra attenuation due to the injected carriers. As before, rejections better than −35 dB on the rejected channels at through output and crosstalks lower than −37 dB at the drop channel outputs are obtained. This crosstalk is only for the next stage side channel, the previous stage side channel after the first *on* state switch, have a crosstalk of −37 dB less than the attenuation of 35 dB, this is 72 dB, as it can be seen in Figs. 12(b) and 13(f). Again the *on* state drop outputs have a FWHM of 16.2 GHz.

5. Conclusions

A polarization independent reconfigurable optical 1xN demultiplexer with low crosstalk between adjacent channels is designed on silicon on insulator technology. On to off state transitions can be implemented by changing the coupling factor or the ring length. Wavelength selective switch units, based on a Michelson configuration embedded on a Ring Resonator are cascaded to form the demultiplexer. Designs using carrier dispersion effect and power consumption estimations are included. Crosstalks below −30dB with 50GHz channel spacing and losses below 1.5dB in the off state are obtained for a 1x4 demultiplexer. Rejection ratio between the two states is 26 dB. Drop channels with Full Width at Half Maximum of 16 GHz are obtained. Power consumption could be reduced using other coupling techniques based on micro-electromechanical technologies or optomechanical oscillators.

Acknowledgments

This work has been sponsored by the Spanish Economy and Education Ministries through grants (Ref.TEC2012-37983-C03-02) and by a SENACYT grant given to one of the authors. We thank to Dr. Dimitrios Zografopulos for his helpful discussions.